

Brownian dynamics simulations of charge mobility on conjugated polymers in solution

Nicolae M. Albu and David J. Yaron

Department of Chemistry, Carnegie Mellon University, Pittsburgh, PA 15213

Keywords: Brownian dynamics, mobility of conjugated polymers

A model is developed for the mobility of a charge carrier along a conjugated polymer dissolved in solution, as measured by time-resolved microwave conductivity. Each unit cell of the polymer is assigned a torsional degree of freedom, with Brownian dynamics used to include the effects of solvent on the torsions. The barrier to torsional motion is substantially enhanced in the vicinity of the charge, leading to self trapping of the charge onto a planarized region of the polymer chain. Within the adiabatic approximation used here, motion arises when regions of the polymer on either side of the charge fluctuate into planarity and the wavefunction spreads in the corresponding direction. Well-converged estimates for the mobility are obtained for model parameters where the adiabatic approximation holds. For the parameters expected for conjugated polymers, where crossing between electronic surfaces may lead to breakdown in the adiabatic approximation, estimates for the mobility are obtained via extrapolation. Nonadiabatic contributions from hopping between electronic surfaces are therefore ignored. The resulting mobility is inversely proportional to the rotational diffusion time, t_{rot} , of a single unit cell about the polymer axis in the absence of intramolecular forces. For t_{rot} of 75 ps, the long-chain mobility

of poly(*para*-phenylene vinylene) is estimated to be between 0.09 and 0.4 cm^2/Vs . This is in reasonable agreement with experimental values for the polymer, however, the nonadiabatic contribution to the mobility is not considered, nor are effects arising from stretching degrees of freedom or breaks in conjugation.

I. Introduction

Conjugated polymers are a useful class of materials for constructing plastic electronic devices¹. For many applications, such as field effect transistors, the charge mobility plays an important role in establishing device performance. The mobility of direct relevance to devices is that in thin films, which is likely strongly influenced by structural disorder and the need for charges to hop between polymer chains in order to move substantial distances. Nevertheless, the charge mobility along a single polymer chain is of fundamental interest, since it establishes the inherent conductivity of a conjugated polymer. The mobility on single polymer chains can be measured in solution through time-resolved microwave conductivity (TRMC)². The computations presented here explore the factors that contribute to establishing this solution-phase mobility.

Current theoretical models of solution-phase mobility use the time-dependent Schrödinger equation to propagate the charge along a polymer chain²⁻⁶. For poly(*para*-phenylene vinylene) (PPV), and microwaves with a frequency of 34 GHz, such models estimate the mobility to be about 60 cm^2/Vs on a long chain. This is considerably larger than the experimental value of 0.46 cm^2/Vs measured for PPV polymer. The lower value seen experimentally has been attributed to the limited length of well conjugated regions within the polymer. Simulations on oligomers and polymers with intentionally introduced defects find good agreement with

experiment, supporting the notion that limited chain lengths strongly influence the measured mobilities.

By using the time dependent Schrödinger equation to propagate the wavefunction describing the charge, the existing models take as their starting point the coherent motion of the charge along the chain. Electronic dephasing is present in such models through a number of sources. One such source is structural disorder, which is included by averaging over an ensemble of structures whose torsional disorder reflects that expected for a Boltzmann distribution at the experimental temperature. Another source of dephasing is motion in the torsional degrees of freedom, which is included by allowing the torsional degrees of freedom to evolve under the influence of both intramolecular forces and solvent forces.

Here, we use a quantum chemical model of the polymer that is equivalent to that used above²⁻⁶, but start from the opposite extreme of incoherent motion of the charge along the polymer. Within the adiabatic approximation considered here, the motion of the charge can be viewed as follows. Stiffening of the torsional potential in the vicinity of the charge leads to self-trapping of the charge onto a planarized region of the polymer^{7,8}. The mobility then reflects the motion of this planarized region along the chain. The model is sufficiently simple that trajectories may be run for long periods of time, giving well-converged estimates for the mobility.

The use of the adiabatic approximation influences the mechanism through which the charge can move in the computations. The adiabatic approximation is valid when the gap between the ground and first-excited electronic state is sufficiently large. This is the case for model parameters that lead to strong self-trapping of the charge, *i.e.* low barrier to torsion on the uncharged polymer and strong stiffening in the vicinity of the charge. For such parameters, the

mobility arises from solvent fluctuations that cause the planarized region of the chain to drift. We refer to the contribution from this process as the adiabatic contribution to the mobility. As the parameters are adjusted towards the values expected for PPV, the adiabatic approximation begins to break down due to frequent crossing between electronic surfaces. Hopping between electronic surfaces at these crossings would serve to increase the mobility, and we refer to such increases as the non-adiabatic contribution to the mobility. The simulations performed here are limited to the adiabatic contribution. By extrapolating from parameters where the adiabatic approximation holds to the values expected for PPV, we can obtain estimates of the adiabatic contribution to the mobility of PPV. Since hopping between electronic surfaces likely increases the mobility, the adiabatic contribution obtained here correspond to a lower limit on the mobility. Estimates of the enhanced mobility due to surface hopping requires non-adiabatic simulations⁹⁻¹², which are not carried out in the current work.

Section II describes the quantum chemical model used for the charge, the Brownian dynamics used to include effects from the solvent, and the approach used to extract the mobility from the dynamics. Section III examines the predictions of the model, and Section IV discusses these in the context of experiment and past computational modeling.

II. Methods

II-A. Quantum Chemical Model

The polymer is modeled as a chain of N generalized sites (unit cells) of an oligomer, where each site represents one unit cell of the polymer and has a single torsional degree of freedom, θ_i . The torsional potential in the ground state is modeled with a simple molecular mechanical form, written as:

$$E_{gs} = \frac{1}{2}V_{gs} \sum_{i=1}^{N-1} [1 - \cos[2(\theta_{i+1} - \theta_i)]] + \frac{1}{2}V_{gs} [1 - \cos[2(\theta_N - \theta_1)]] \quad (1)$$

where θ_i is the torsional angle of the i^{th} ring, V_{gs} sets the magnitude of the torsional potential, and periodic boundary conditions are assumed. Eq. (1) is the lowest order trigonometric form that has a minimum for the planar structure and a maximum for all rings twisted to 90 degrees.

The wavefunction and energy of the charge are obtained from the following matrix, which assumes coupling between sites that is proportional to the cosine of the angle between sites,

$$\begin{pmatrix} \alpha & \beta \cos(\theta_2 - \theta_1) & & & \beta \cos(\theta_N - \theta_1) \\ \beta \cos(\theta_2 - \theta_1) & \alpha & \beta \cos(\theta_3 - \theta_2) & & \\ & \beta \cos(\theta_3 - \theta_2) & \alpha & \ddots & \\ & & \ddots & \ddots & \beta \cos(\theta_N - \theta_{N-1}) \\ \beta \cos(\theta_N - \theta_1) & & & \beta \cos(\theta_N - \theta_{N-1}) & \alpha \end{pmatrix}. \quad (2)$$

where β sets the magnitude of the coupling between sites, and periodic boundary conditions are assumed. α is the ionization potential of a single site, which has no impact on the model predictions discussed below and so is set to zero.

The position, or center, of the charge is obtained using the following means to handle the periodic boundary conditions.

$$x = \frac{Na}{2\pi} \tan^{-1} \left(\frac{\sum_{i=1}^N c_i^2 \sin\left(\frac{2\pi}{N}i\right)}{\sum_{i=1}^N c_i^2 \cos\left(\frac{2\pi}{N}i\right)} \right) \quad (3)$$

where c_i is the amplitude of the eigenfunction of Eq. (2) on the i^{th} site, and a is the length of a unit cell taken here as 6.6Å to correspond to PPV. Eq. (3) is obtained by assuming the polymer is wrapped into a circle with circumference Na . The angle corresponding to the position of the i^{th}

site is then $(2\pi/N) i$. The numerator and denominator of the fraction in Eq. (3) are the average \sin and \cos of the angular position of the charge, and the sign of the inverse tangent is determined based on the quadrant corresponding to these averaged values.

The quantum chemical model used above is equivalent to that used in previous work on the mobility of charges on isolated polymer chains. For PPV, quantum chemical calculations find β of about -20 kcal/mol , with twisting between the phenyl and vinylene groups having a barrier of about 4.6 kcal/mol ⁵. For polyfluorene, which does not have vinylene groups between conjugated rings, the barrier height is lower, being about 2.3 kcal/mol ¹³. Since we are treating the entire unit cell of PPV as a site, we take a reduced value of $V_{gs} = 2.5 \text{ kcal/mol}$ for the torsional barrier and estimate $\beta = -25 \text{ kcal/mol}$.

The charge is assumed to remain in the state corresponding to the lowest eigenvalue of Eq. (2). This adiabatic approximation is valid over a limited range of model parameters. As discussed in more detail below, the applicability of the adiabatic approximation is tested through computations that limit the number of sites included in the matrix diagonalization. The sites included in the diagonalization correspond to a window of size w centered around the charge. This is implemented in the Brownian dynamics by including, in the matrix diagonalization for each step of the dynamics, only sites that lie within $(w-1)/2$ unit cells of the center of charge, x of Eq. (3), obtained from the previous time step. The window thereby moves with and remains centered on the charge. Section III-A argues that, for cases where the adiabatic approximation holds, the calculated mobility saturates with increasing window size, w . Failure to converge with w is a signature of breakdown in the adiabatic approximation. All calculations of mobility are done on a chain with a total of 100 sites, using various window sizes.

II-B. Brownian Dynamics

To model mobility in solution, we use Brownian dynamics to include solvent effects. In Brownian dynamics, the solvent gives rise to both stochastic forces and friction, via ¹⁴

$$\begin{aligned} \dot{\theta}_i &= v_i \\ \dot{v}_i &= a_i - \gamma v_i + A_i \end{aligned}, \quad (4)$$

where θ_i and v_i are the torsional angle and velocity, respectively, of the i^{th} unit cell, and a_i is the acceleration due to forces calculated as analytical derivatives of the torsional potentials described above,

$$a_i = \frac{1}{I} \frac{dE}{d\theta_i}. \quad (5)$$

Here I is the moment of inertia of a ring, taken as $91.1 \text{ amu} \cdot \text{Å}^2$. The friction coefficient, γ in Eq. (4), is the same for all sites, which assumes that the solvent effects are isotropic and independent of the system configuration. Finally, the random force term, $A_i(t)$ of Eq.(4), is a stochastic Gaussian process given by:

$$\begin{aligned} \langle A_i(t) \rangle &= 0 \\ \langle A_i(t) A_j(0) \rangle &= \delta_{ij} \cdot 2\gamma \frac{k_B T}{I} \cdot \delta(t) \end{aligned} \quad (6)$$

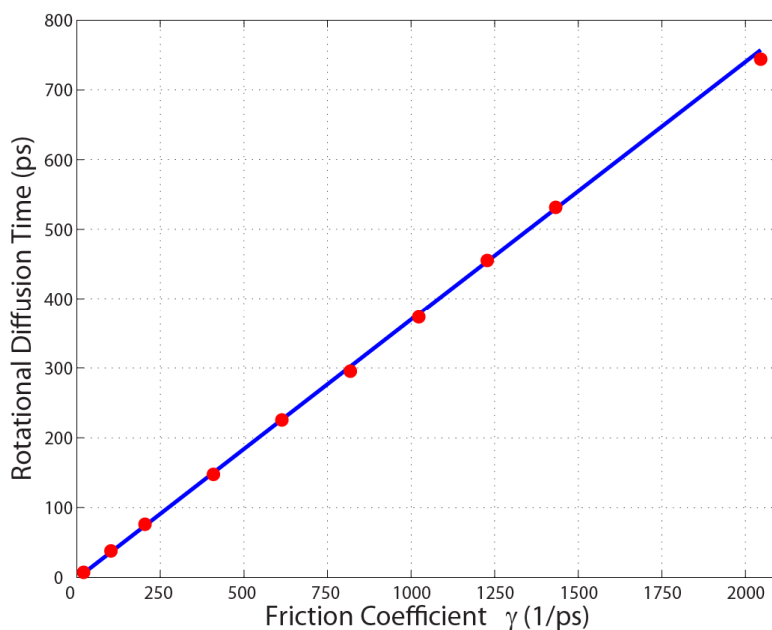


Figure 1 Linear dependency of the rotational diffusion time of a single ring on the friction coefficient of Eq. (4).

The random force is related to the solvent friction by the fluctuation-dissipation theorem, such that the model contains only one parameter, γ , which defines the nature of the solvent. Rather than quote the value of γ below, we quote the rotational diffusion time, t_{rot} , of a single unit cell that arises from the solvent in the absence of any intramolecular forces. Note that this is the diffusion time for rotation of a unit cell about the polymer axis, as opposed to the rotational diffusion time of a free unit cell in solution. The relation between γ and t_{rot} is linear, as shown in Figure 1. Most of the results shown below are obtained with $t_{rot} = 7.5$ ps. The results scale with t_{rot} , allowing predictions to be easily made for other values. For polymers with side chains, t_{rot} has been estimated as lying between 30 and 200 ps²⁻⁵, and we will take $t_{rot} = 75$ ps as a representative value.

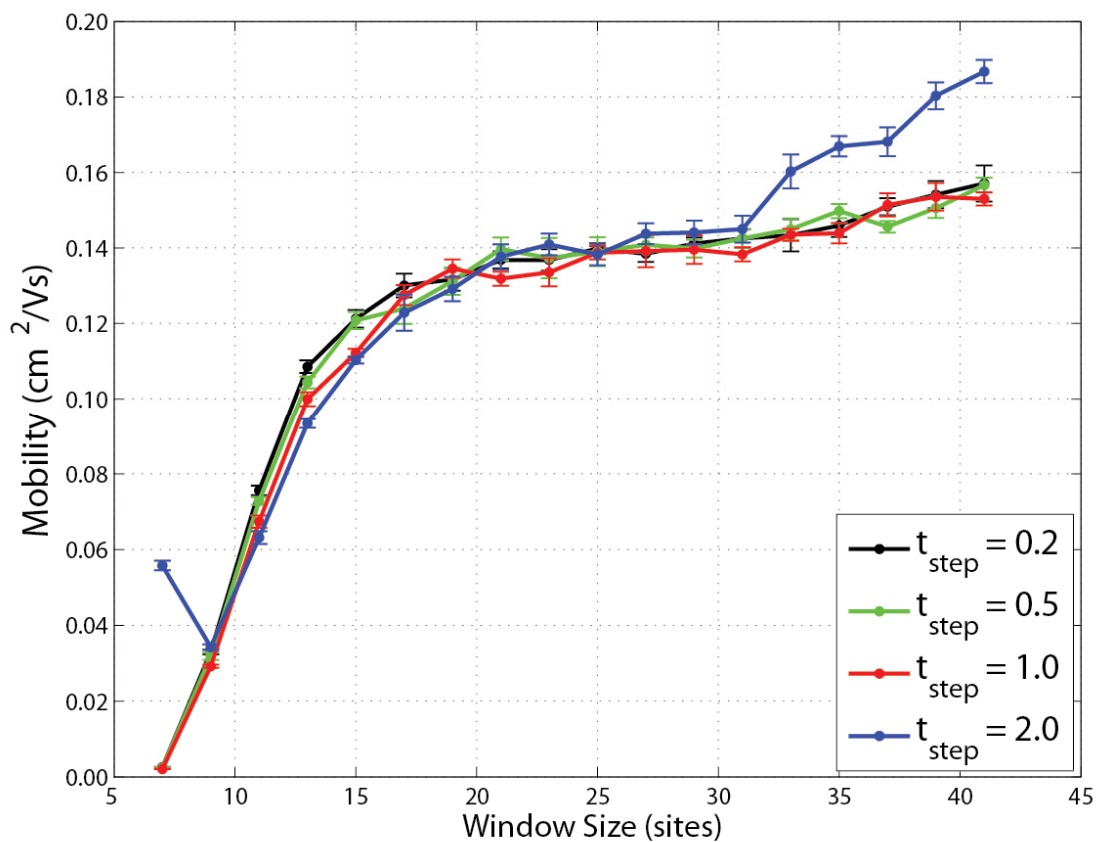


Figure 2 Mobility as a function of window size obtained for various integration time steps (t_{step} is given as multiples of 48.8 fs). Results are for a chain with 100 sites, with $V_{gs} = 0$, $\beta = -70$ kcal/mol and $t_{rot} = 7.5$ ps.

The integration time step used for the Brownian dynamics is 48.8 fs when $t_{rot} = 7.5$ ps. This time step, $0.0064 t_{rot}$, was chosen based on the results of Figure 2, which shows that decreasing the integration step by a factor of 2 and 5 does not alter the predictions. For other values of t_{rot} , we use a more conservative time step of $0.0032 t_{rot}$, to ensure that dependence on t_{rot} is well described.

II-C. Calculation of Mobility

The mobility is obtained from the random walk of the charge along the chain. The fluctuation-dissipation theorem allows us to relate mean square displacement of this random walk to mobility via⁶

$$\mu = \frac{-e \omega^2}{2k_B T} \operatorname{Re} \left[\int_0^{\infty} \langle x^2(t) \rangle e^{-i\omega t} dt \right], \quad (7)$$

where μ is the mobility at frequency ω , T is temperature, k_B is the Boltzmann constant, and e is the electron charge. $\langle x^2(t) \rangle$ is the mean square displacement obtained from the trajectory,

$$\langle x^2(t) \rangle = \langle (x(t) - x(0))^2 \rangle = \frac{1}{t_{\text{traj}} - t} \int_0^{t_{\text{traj}} - t} d\tau (x(\tau + t) - x(\tau))^2. \quad (8)$$

Periodic boundary conditions are taken into account when evaluating $x(\tau + t) - x(\tau)$. If the random walk is a Markovian process, then the mean square displacement increases linearly in time such that

$$\langle x^2(t) \rangle = 2Dt, \quad (9)$$

where D is the diffusion constant. Insertion of Eq. (9) into Eq. (7) gives

$$\mu = \frac{-e \omega^2}{2k_B T} \operatorname{Re} \left[\int_0^{\infty} 2Dt e^{-i\omega t} dt \right] = \frac{eD}{k_B T} \quad (10)$$

An estimate of the mobility can therefore be obtained via

$$\mu = \frac{e}{k_B T} \left[\frac{\langle x^2(t) \rangle}{2t} \right] \quad (11)$$

where $\langle x^2(t) \rangle$ is obtained from the Brownian dynamics trajectories via Eq. (8). Each Brownian dynamics trajectory is run for a total of 10^6 time steps, of which the first 5000 steps are an

equilibration phase that is not included in evaluation of Eq. (8). Between 7 and 15 independent trajectories are generated for each set of model parameters, and the results presented below show the mean of the values obtained from these trajectories, with error bars indicating the standard deviation of this mean.

Note that Eq. (11) applies only for a Markovian process. The time scale beyond which the motion of the charge becomes Markovian is obtained by determining the time beyond which $\langle x^2(t) \rangle$ becomes proportional to t , or equivalently, the value of t beyond which the mobility

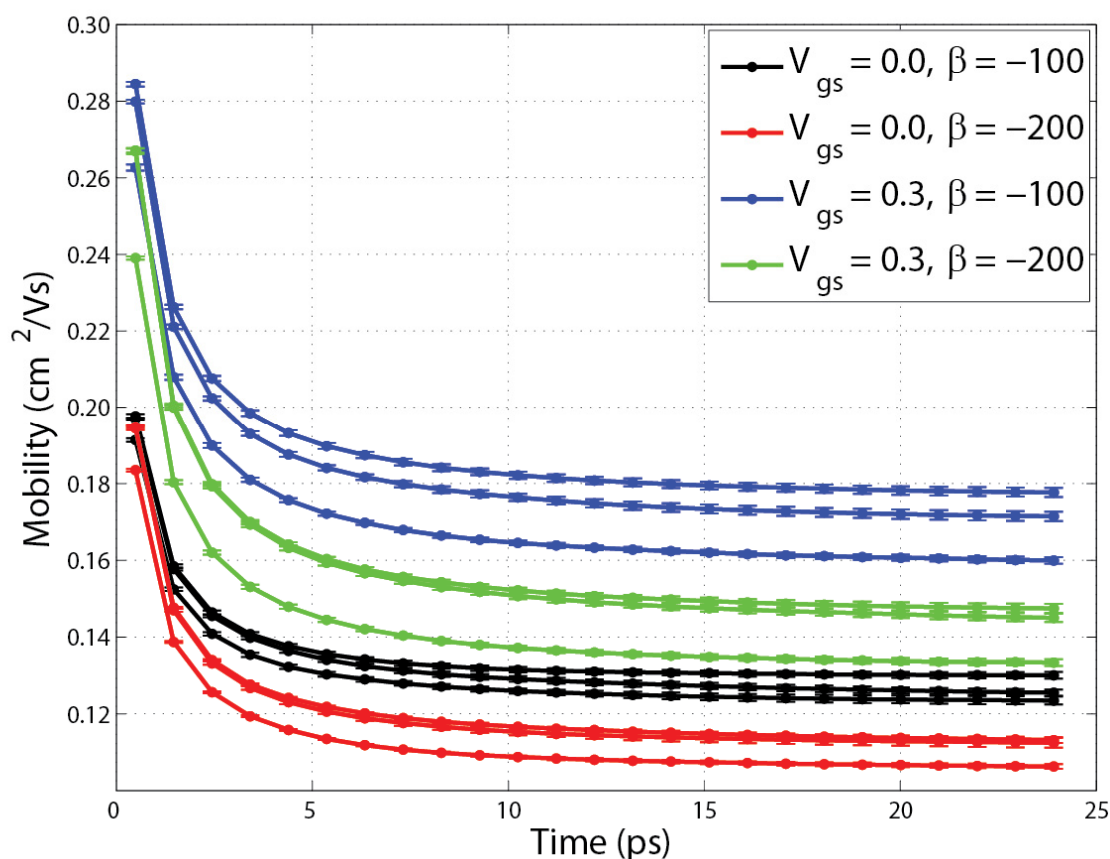


Figure 3 Mobility as a function of the time used to determine the mean square displacement of the charge (Eq. (11)), for $t_{rot} = 7.5$ ps. The three lines shown for each set of parameters correspond to window sizes of 21, 31 and 41 (from bottom to top). The time beyond which the mobility stabilizes indicates the time scale beyond which the motion of the charge becomes Markovian. β and V_{gs} are given in kcal/mol.

estimated from Eq. (11) becomes independent of t (Figure 3). Results are shown for a range of values of V_{gs} and β over which the adiabatic approximation holds and for three different window sizes, w (see Section II-A). Figure 3 shows that the estimated mobility stabilizes beyond about 15 ps , or $2 t_{rot}$, for each set of parameters. This indicates that the motion of the charge corresponds to a Markovian process beyond about $2 t_{rot}$. Equivalently, the motion of the charge is a random walk with uncorrelated jumps, provided a jump is defined as the change in the location of the charge arising for a time step of $2 t_{rot}$ or longer. In the remainder of the paper, the mobilities reported use $t = 100 ps$ in Eq. (11) for $t_{rot} = 7.5 ps$, or more generally $t = 13.3 t_{rot}$.

The effects of the deviation of $\langle x^2(t) \rangle$ from being a linear function of t can be explored using the following functional form,

$$\langle x^2(t) \rangle = 2Dt \left(1 + c_M e^{-\omega_M t} \right), \quad (12)$$

where c_M and ω_M characterize the exponential decay seen in Figure 3. Inserting Eq. (12) into Eq. (7) gives

$$\mu = \mu_{\omega=0} \left(1 + c_M \frac{(\omega / \omega_M)^4 - (\omega / \omega_M)^2}{\left(1 + (\omega / \omega_M)^2 \right)^2} \right), \quad (13)$$

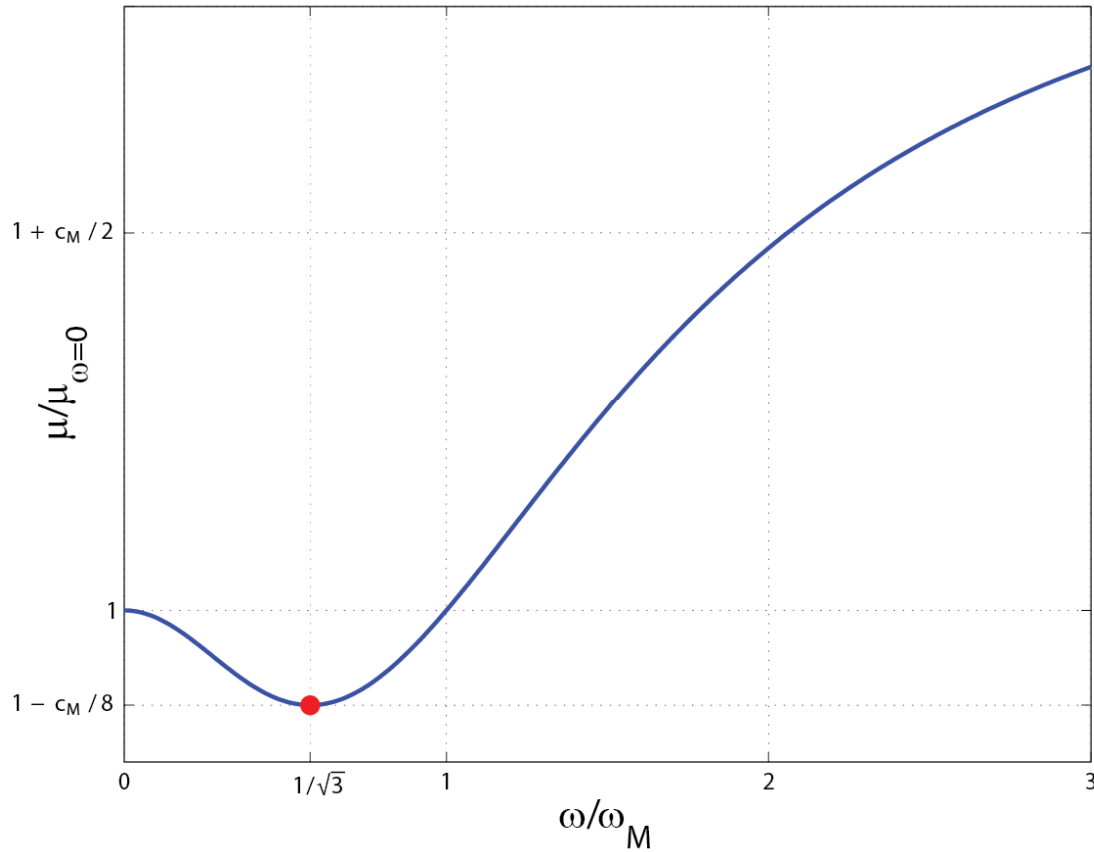


Figure 4 Frequency dependence of the mobility, from Eq. (13), with minimum shown as a red dot.

where $\mu_{\omega=0}$ is the mobility at zero frequency. Figure 4 shows that the frequency dependence reduces the mobility below ω_M , with a minimum value of $(1 - c_M/8)$, and enhances the mobility above ω_M , with a high frequency limit of $1 + c_M$. For the data of Figure 3, where $t_{rot} = 7.5$ ps, ω_M is about 500 GHz and c_M is about 1. Below, we show that t_{rot} establishes the time scale of the simulation, such that for $t_{rot} = 75$ ps, ω_M is about 50 GHz. Near the experimental frequency of 30 GHz, we expect a small frequency dependence that reduces the mobility from the zero-frequency result by less than 15%. Defects that limit the effective conjugation length may also contribute to the frequency dependence⁴.

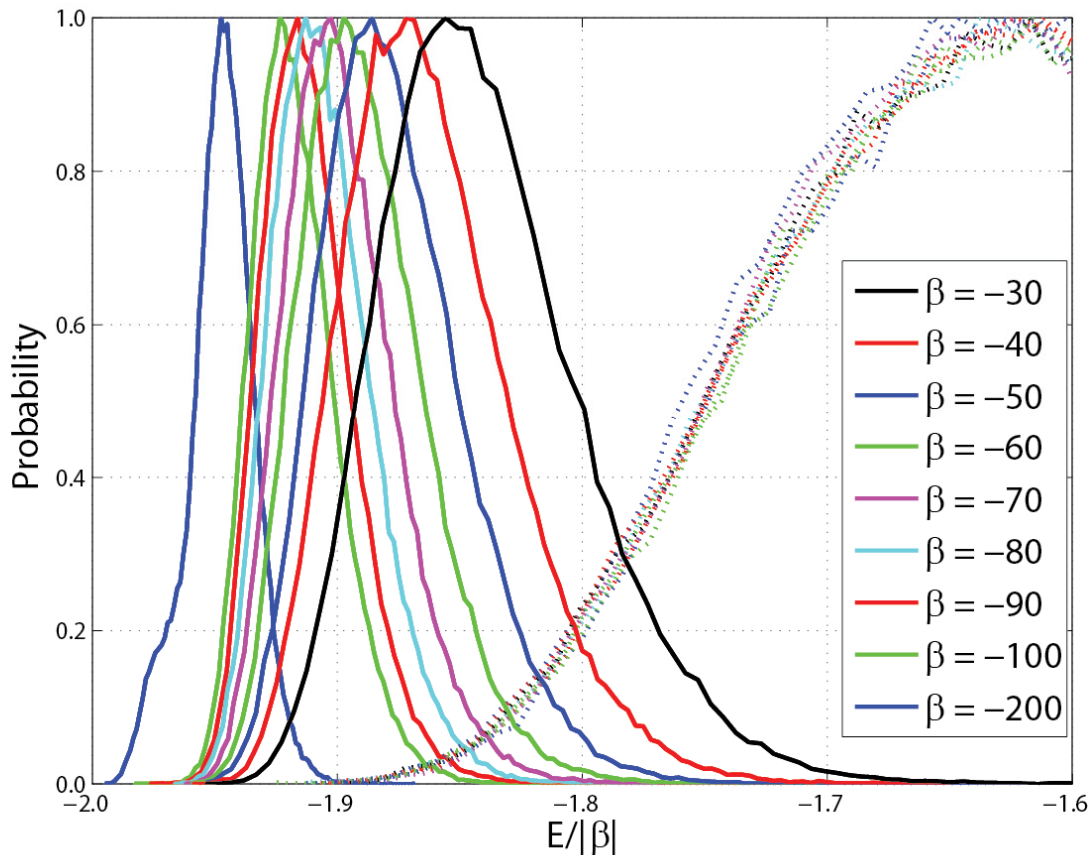


Figure 5 Energy distribution of a charge on a chain with 20 sites (solid lines), and distribution of energy required to create a charge on an initially uncharged chain with 20 sites (dotted lines). Substantial overlap of these distributions leads to breakdown in the adiabatic approximation. $V_{gs} = 0$, $t_{rot} = 7.5$ ps, and β is in kcal/mol.

III. Results

III-A. Range of validity of the adiabatic approximation

In the Brownian dynamics simulations, the lowest-energy eigenstate of the matrix in Eq. (2) is used to calculate the position of the charge, x of Eq.(3), and the forces associated with the torsional angles in Eq. (5). This is valid provided the energy gap to the next highest energy state is sufficiently large. The impact of breakdown in the adiabatic approximation can be understood

by consider a simulation involving two uncoupled chains, only one of which is charged. Given the absence of coupling between the chains, any hop of the charge between chains is a clear artifact of breakdown in the adiabatic approximation. Since the adiabatic approximation selects electronic states based only on their energy, such hops will occur whenever the fluctuations are such that the charge could lower its energy by hopping from the currently charged chain to the currently uncharged chain. Figure 5 shows the energy distributions relevant to determining the likelihood of such fluctuations. The solid lines show the energy distribution corresponding to the charged chain. The dotted lines show the energy associated with creating a charge on the uncharged chain. When there is substantial overlap between these two energy distributions, fluctuations will often lead to situations where the charge can lower its energy by jumping between chains. In adiabatic dynamics, such jumps are allowed despite the lack of coupling between chains. This gives insight into the artifacts that may arise in adiabatic dynamics on long chains. The lower average energy and smaller fluctuations obtained on the charged chain reflects self-trapping of the charge onto a planarized region of the chain. When this energy distribution has substantial overlap with the distribution of energies required to create a charge on an uncharged chain, adiabatic dynamics will lead to frequent jumps from the planarized region associated with the self-trapped charge to remote regions of the chain that have spontaneously fluctuated into a more planar configuration.

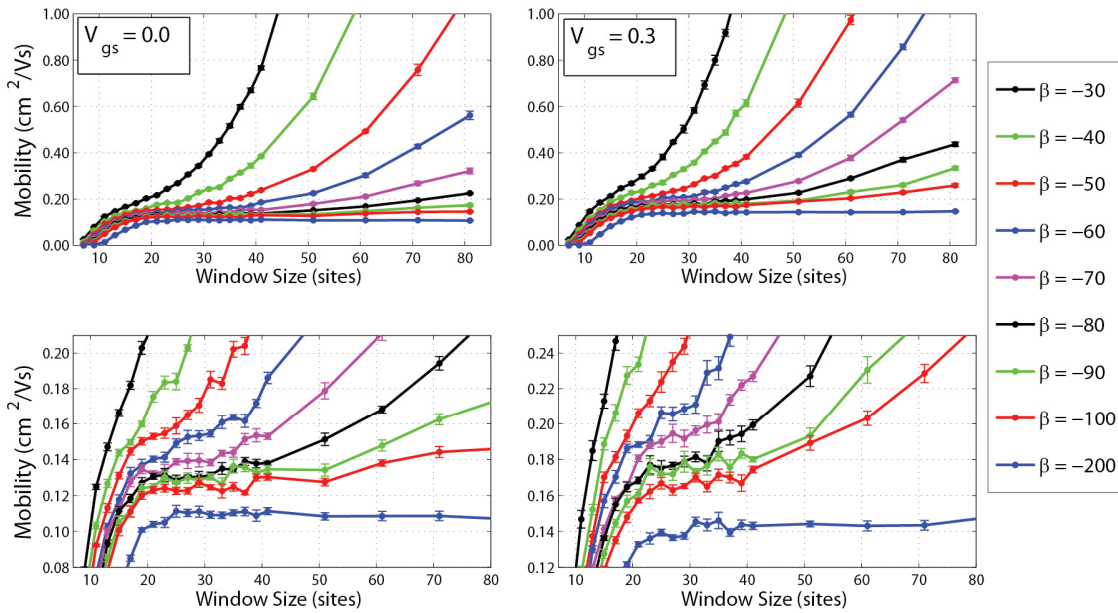


Figure 6 Mobility as a function of window size for $V_{gs} = 0$ (left panels) and $V_{gs} = 0.3$ kcal/mol (right panels). The lower panels are detailed views of the data in the upper panels. Units for β are kcal/mol, and $t_{rot} = 7.5$ ps.

To monitor the occurrence of such artifactual, long-range, jumps, we examine the computed mobility as a function of the window size, w , within which we diagonalize the matrix of Eq. (2). For $V_{gs} = 0$ and $\beta = -200$ kcal/mol, where there is little overlap of the energy distributions in Figure 5, the mobility increases with w and saturates by about 21 sites (Figure 6). The initial increase with window size reflects the size of the self-localized charge. For w beyond about 21 sites, increasing the window size has little effect on the mobility because the wavefunction of the charge remains localized to less than this number of sites. (Recall that, at each integration step, the center of the window is adjusted to the center of the charge from the previous step. The window therefore follows the motion of the charge.) For cases where the mobility saturates with w , the charge moves because sites on either side of the charge fluctuate into planarity and the wavefunction spreads in that direction. We will refer to this mechanism as

adiabatic motion of the charge, and the resulting mobility as the adiabatic contribution to the mobility.

When the magnitude of β is lowered to $\beta = -30 \text{ kcal/mol}$, there is substantial overlap between the energy distributions in Figure 5. For these parameters, the mobility rises rapidly with window size, w . This indicates that the charge is hopping rapidly between electronic surfaces and non-adiabatic dynamics would be required to obtain a reliable estimate of the mobility. For the intermediate value of $\beta = -70 \text{ kcal/mol}$, we see a plateau between about $w = 21$ and $w = 41$ sites. We can rationalize this as follows. The initial rise to the plateau reflects the size of the localized charge. Within the plateau region, the portion of the chain that is within the window, but unoccupied by the charge, is not sufficient to support a lower-energy location for the charge. Beyond the plateau, remote lower-energy locations begin to appear within the window and the adiabatic approximation leads to artifactual jumps to these remote regions. Such jumps may indeed occur and contribute to the mobility, however, the adiabatic algorithm overestimates the occurrence of such jumps and so does not provide a reliable estimate of their contribution to the mobility. We will refer to the contribution of such jumps as the non-adiabatic contribution to the mobility. The value of the mobility on the plateau is taken as an estimate of the adiabatic contribution to the mobility, which provides a lower-limit to the actual mobility.

The adiabatic approximation holds for parameters corresponding to strong self-trapping of the charge. The degree of self-trapping increases with $|\beta|$. The degree of self-trapping decreases as V_{gs} is increased, such that for $V_{gs} = 0.3 \text{ kcal/mol}$, a larger magnitude of β is required for the adiabatic approximation to hold (right panels of Figure 6).

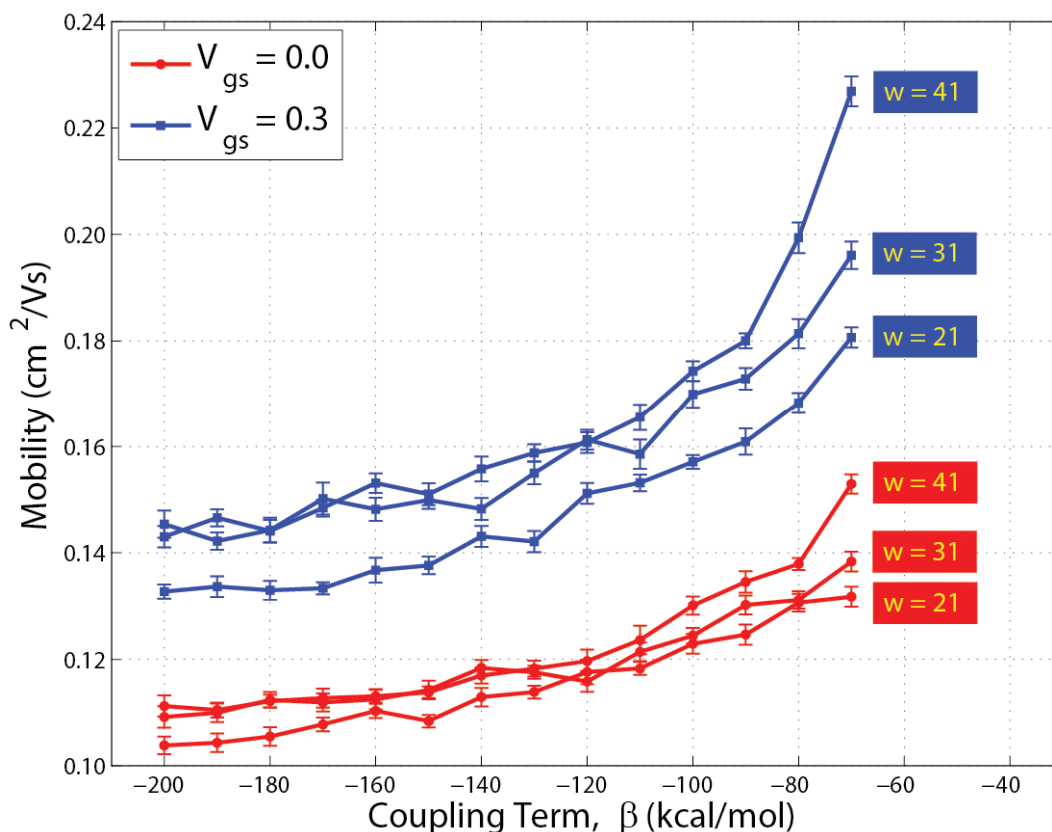


Figure 7 Extrapolation of mobility to lower magnitude values of β . Comparison of window sizes 21, 31, and 41 is used to evaluate the existence of a plateau in the dependence of mobility on window size (Figure 6), and thus the ability to estimate the adiabatic contribution to the mobility. Units for V_{gs} are *kcal/mol*, and $t_{rot} = 7.5$ ps.

III-B. Dependence of mobility on model parameters

For parameters over which the adiabatic approximation holds, the dependence of the mobility on model parameters can be obtained. Given this dependence, we may then extrapolate to values of the parameters for which the adiabatic approximation breaks down. This extrapolation can be used to estimate the adiabatic contribution to the mobility. As discussed above, the applicability of the adiabatic approximation is related to the existence of a plateau in the plot of mobility versus window size. Figure 7 shows a plot of mobility versus β , obtained with window sizes of 21, 31 and 41. For $V_{gs} = 0$, the results obtained for windows of 21, 31 and 41 agree well for $|\beta|$ greater than about 80 *kcal/mol*, in agreement with the values of $|\beta|$ for which a plateau is seen in Figure 6. For $V_{gs} = 0.3$, comparison of windows 21, 31 and 41 indicate a plateau for $|\beta|$ greater

than about 100 kcal/mol , also in agreement with Figure 6. For both of these values of V_{gs} , the dependence on β is relatively weak. For $V_{gs} = 0$, a rough extrapolation to the expected PPV value of about $\beta = -25 \text{ kcal/mol}$ (Section II-A) gives a mobility of $0.17 \text{ cm}^2/Vs$. For $V_{gs} = 0.3 \text{ kcal/mol}$, the extrapolation depends on whether one attributes the steeper rise below $|\beta|$ of 100 kcal/mol to an actual dependence on β or to breakdown in the adiabatic approximation (as indicated by the increasing dependence of the results on window size). Due to this uncertainty, extrapolation of the mobility to $\beta = -25 \text{ kcal/mol}$ gives a range of values, 0.2 to $0.3 \text{ cm}^2/Vs$. Below, extrapolation from $\beta = -150 \text{ kcal/mol}$ to $\beta = -25 \text{ kcal/mol}$ will be taken as increasing the mobility by a factor of between 1.5 and 2.

Figure 8 shows the predicted mobility as a function of V_{gs} from 0 to 1 $kcal/mol$. For $\beta = -100$ $kcal/mol$, the adiabatic approximation begins to breakdown beyond about $V_{gs} = 0.8$ $kcal/mol$, as indicated by large deviations between the values obtained for different window sizes. For $\beta = -150$ $kcal/mol$, the adiabatic approximation holds up to about $V_{gs} = 1$ $kcal/mol$. Rough extrapolation of the $\beta = -150$ $kcal/mol$ results from $V_{gs} = 1$ $kcal/mol$ to the PPV value of $V_{gs} = 2.5$ $kcal/mol$ (Section II-A), gives a predicted mobility of between 0.75 and 2 cm^2/Vs , corresponding to increase by a factor of between 2 and 7.

To extrapolate across both V_{gs} and β , we begin with the mobility of 0.3 cm^2/Vs obtained

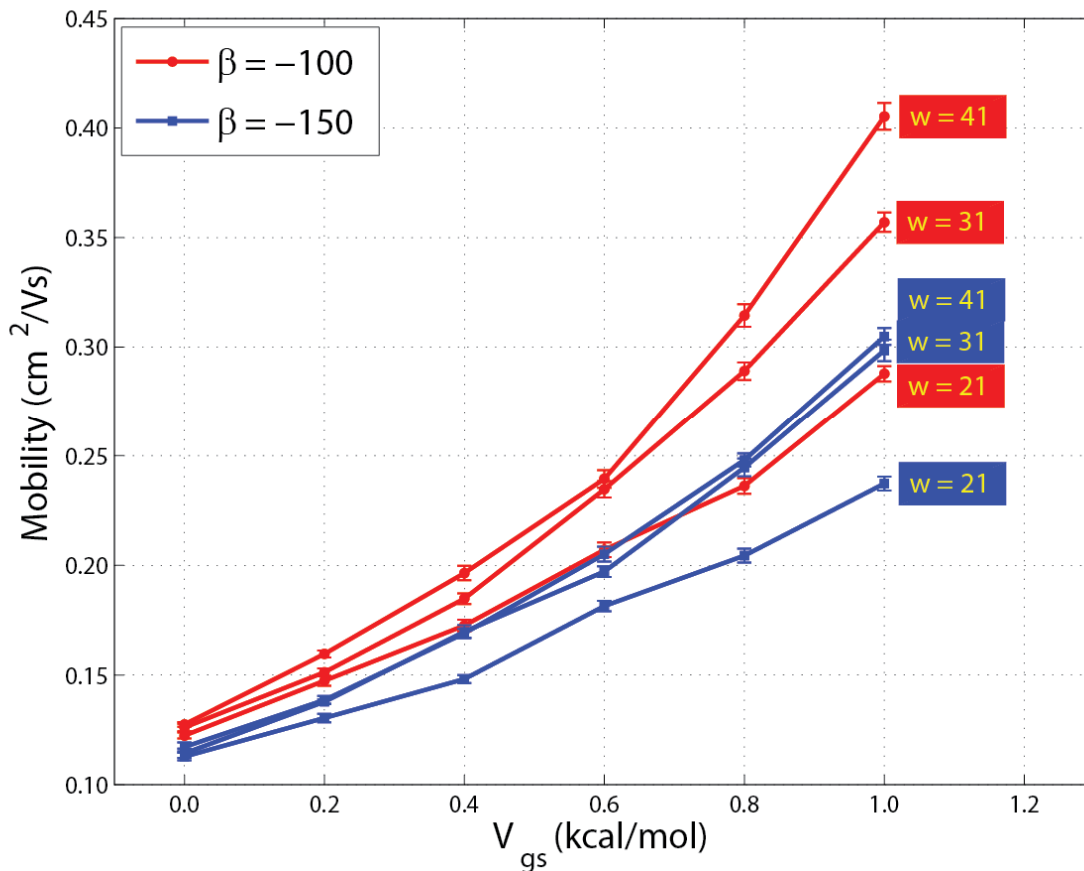


Figure 8 Extrapolation of mobility to larger values of V_{gs} , in a manner similar to that of Figure 7. Units for β are $kcal/mol$, and $t_{rot} = 7.5$ ps .

for $V_{gs} = 1 \text{ kcal/mol}$ and $\beta = -150 \text{ kcal/mol}$, where the good agreement between $w=31$ and 41 in Figure 8 indicates a good plateau region and therefore a reliable estimate of the adiabatic contribution to the mobility. Extrapolation from $\beta = -150 \text{ kcal/mol}$ to $\beta = -25 \text{ kcal/mol}$ increases the mobility by a factor of between 1.5 and 2. Extrapolation from $V_{gs} = 1$ to 2.5 kcal/mol increases the mobility by a factor of between about 2 and 7. Combining these gives a factor of 3 to 14, or an extrapolated mobility between about 0.9 and $4 \text{ cm}^2/Vs$ for $t_{rot} = 7.5ps$, with most of the uncertainty coming from the extrapolation in V_{gs} .

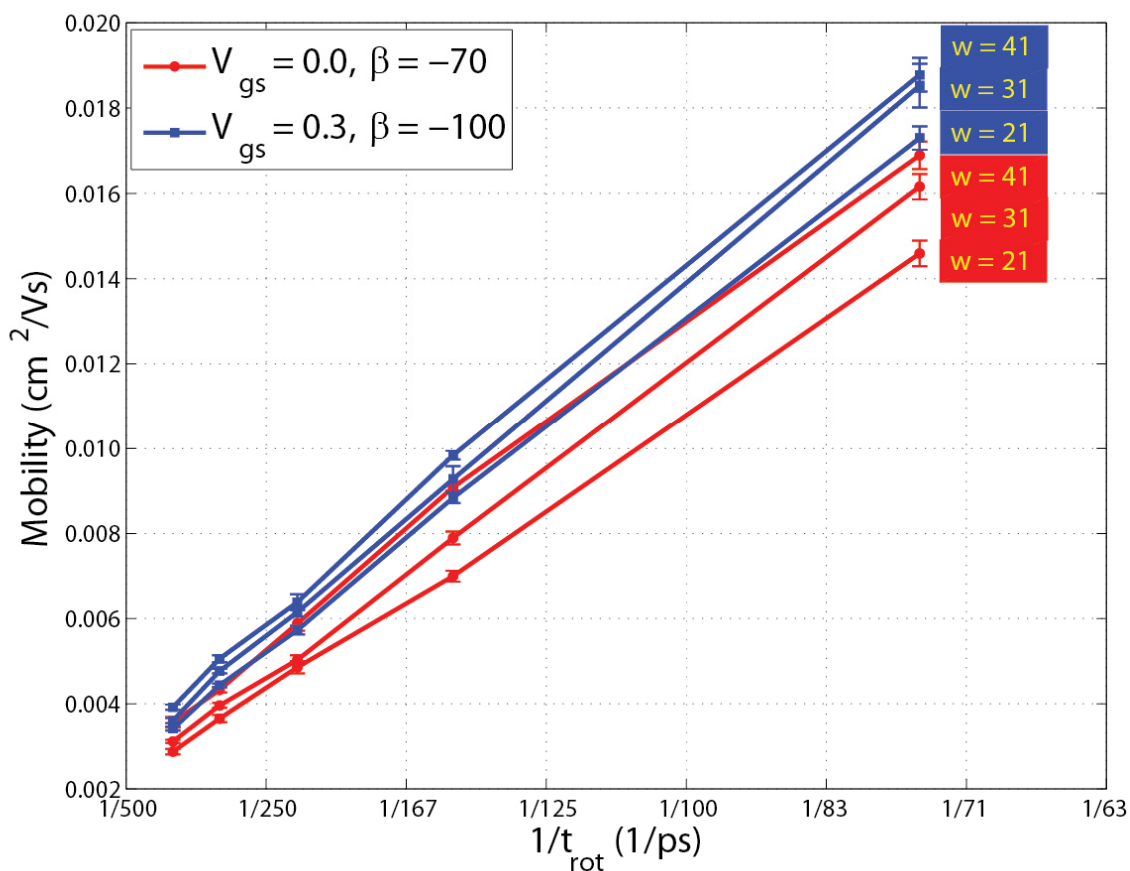


Figure 9 Dependence of the mobility on the rotational diffusion time of an isolated ring of the polymer, t_{rot} . Units for β and V_{gs} are kcal/mol .

Finally, we consider the dependence on t_{rot} . Figure 9 shows that the mobility is proportional to $1/t_{rot}$. Taking $t_{rot}=75$ ps reduces the above estimate for the mobility of PPV by one order of magnitude, or 0.09 to 0.4 cm^2/Vs .

IV. Discussion

The computational approach used here is able to obtain well-converged results for the mobility within the adiabatic approximation. This approximation holds for parameters corresponding to strong self trapping of the excitation onto a planarized region of the polymer, i.e. low torsional barriers in the ground electronic state, V_{gs} , and strong coupling of charge between sites, β . In this limit, the mobility is most sensitive to the nature of the solvent-solute interactions, as captured by t_{rot} , the rotational diffusion time of a single aromatic ring of the polymer in the absence of intramolecular forces. t_{rot} sets the time scale for the dynamics, such that the mobility is inversely proportional to t_{rot} . Taking $t_{rot}=75$ ps yields a mobility of 0.03 cm^2/Vs for $V_{gs} = 1$ $kcal/mol$ and $\beta = -150$ $kcal/mol$, parameters for which the adiabatic approximation holds. Examination of the dependence of the mobility on β suggests that extrapolation to -25 $kcal/mol$, the value expected for PPV, increases the mobility by a factor of between 1.5 and 2. For V_{gs} , extrapolation to the 2.5 $kcal/mol$ value expected for PPV increases the mobility by a factor of between 2 and 7. The combined extrapolation therefore gives an estimated range of 0.09 to 0.4 cm^2/Vs for the mobility of PPV. The strong dependence on t_{rot} and V_{gs} is consistent with a physical picture for motion of the planarized region holding the charge, in which the charge moves because sites on either side of the current location fluctuate into planarity and the wavefunction spreads in the corresponding direction.

The mobility extracted from TRMC experiments on PPV is $0.46 \text{ cm}^2/Vs$ at 34 GHz , in reasonable agreement with the range predicted here. However, direct comparison with experiment is complicated by a number of factors. First is the use of the adiabatic approximation in the above computations. For the parameters appropriate for PPV, there are frequent crossings of electronic surfaces and hopping between these surfaces would serve to increase the mobility. The extrapolations performed here attempt to isolate the adiabatic contribution to the mobility by assuming that the dependence on parameters in Figure 7 and Figure 8 holds beyond the range where the computations were performed. No attempt is made here to estimate the non-adiabatic contribution to the mobility.

The second factor that complicates comparison with experiments is the assumption of an unlimited chain length. Past computations obtain substantially higher estimates for the mobility of a long chain, $60 \text{ cm}^2/Vs$, and attribute the reduced value seen experimentally to the limited length of well-conjugated segments in the polymer^{2,4}. Here, the predicted long-chain mobility is much smaller, about $0.2 \text{ cm}^2/Vs$. Using $t = 30 \text{ ps}$ in Eq. (11), corresponding to the period of a 34 GHz microwave, gives $\sqrt{\langle x^2(t) \rangle}$ of about 8 unit cells for $\mu = 0.2 \text{ cm}^2/Vs$ and 140 unit cells for $\mu = 60 \text{ cm}^2/Vs$. This suggests that, for the low long-chain mobility predicted here, defects that serve to shorten the effective chain length of the polymer may not have a major impact on the measured mobility.

The means through which the charge moves in the model considered here is somewhat different than that of past computations and this leads to differences regarding the predicted dependence on model parameters. Here, the mobility is strongly influenced by t_{rot} , since the charge moves when sites on either side of the current location of the charge fluctuate into planarity with the charged region. The fluctuations induced by the solvent are then the primary

driving force for charge motion. In wavepacket propagation, the role of rotational diffusion is to enhance mobility by removing twists near 90° that restrict charge motion⁵. This leads to a weaker dependence on t_{rot} , such that changing t_{rot} from 10 to 100 *ps* changes the mobility by less than a factor of 4^5 , as opposed to the factor of 10 predicted here based on the inverse relationship between μ and t_{rot} . The dependence on the charge coupling, β , is also quite different in the two models. In wavepacket propagation, the mobility is directly proportional to the magnitude of β , as expected for band-like transport. In Figure 7, the dependence is much weaker and in the opposite direction.

The large disagreement between the mobility predicted here and that obtained from wavepacket propagation may arise from a number of factors. One factor is the large difference in time scales of the two computational approaches. In the wavepacket propagation methods, t_{rot} is taken as about 60 *ps* and a few hundred simulations are run, each with a length of about 25 *ps*^{3,5}. The resulting $\langle x^2(t) \rangle$ is found to rise rapidly for about 1 *ps* and then enter a diffusive region where the motion is influenced by disorder in the torsional angles. For the simulations performed here, the time scales are considerably longer. With $t_{rot} = 75$ *ps*, the equilibration time for the trajectory is 2.5 *ns* and the total length is 500 *ns*. Between 7 and 15 such trajectories are needed to obtain estimates for the mobility that have the error bars shown throughout the above Figures. In other work¹⁵, we have examined the time needed for the charge to equilibrate on the chain, and found that relaxation of an initially created charge has two time components, $0.15 t_{rot}$ and $0.025 t_{rot}$, corresponding to 2 *ps* and 12 *ps* for $t_{rot} = 75$ *ps*. Given the 12 *ps* time component involved in the self trapping, and the long trajectories needed here to obtain converged estimates for the mobility, it seems likely that the two simulation approaches are examining different phenomena. Here, we equilibrate the system for 2.5 *ns*, and then examine the motion of the self-

trapped charge. In the wavefunction propagation approach, the simulation time is just beyond that needed for the charge to self-trap and much less than would be needed to obtain converged statistics for the motion of the self-trapped charge. On the other hand, the simulations performed here employ the adiabatic approximation and so may exclude effects that are contained in the wavefunction propagation approach.

Finally, we note that in addition to torsional degrees of freedom, stretching degrees of freedom contribute to self-trapping of the charge^{7,8}. As the barrier to torsions, V_{gs} , is increased, the degree of localization due to torsions will decrease such that inclusion of stretching degrees of freedom becomes essential. In particular, the current model is inapplicable to ladder polymers, where the torsions are nearly frozen.

In summary, this paper considers a model for the mobility of conjugated polymers in solution that includes self-trapping of the charge, due to torsional degrees of freedom, and fluctuations due to interactions with the solvent. The results provide reliable estimates of the mobility for parameters where the adiabatic approximation holds. Extrapolation to parameters appropriate for polymers gives mobilities that are in reasonable agreement with experiment. This agreement may indicate that the mobility in polymers is primarily established by the adiabatic motion modeled here. However, the contribution of nonadiabatic effects to the mobility remain to be considered, as are the influence of factors such as self-trapping due to stretching degrees of freedom and the limited chain length present in actual polymers.

Inclusion of non-adiabatic effects is needed to better understand the factors that establish the mobility. Since the degree to which the adiabatic approximation breaks down may be controlled by varying the parameters, this model may provide a useful system in which to develop and test approaches to nonadiabatic dynamics.

ACKNOWLEDGMENT

Work supported in part by the National Science Foundation (Grants 0719350 and 1027985). The authors thank Xiaochen Cai for early contributions to this work.

- ¹ T.A. Skotheim and J. Reynolds, editors, *Conjugated Polymers: Theory, Synthesis, Properties, and Characterization (Handbook of Conducting Polymers, Third Edition)* (CRC Press, 2006).
- ² F.C. Grozema and L.D.A. Siebbeles, *Journal of Physical Chemistry Letters* **2**, 2951 (2011).
- ³ P. Prins, F.C. Grozema, and L.D.A. Siebbeles, *The Journal of Physical Chemistry. B* **110**, 14659 (2006).
- ⁴ P. Prins, F.C. Grozema, J.M. Schins, and L.D.A. Siebbeles, *Physica Status Solidi (b)* **243**, 382 (2006).
- ⁵ P. Prins, F.C. Grozema, and L.D.A. Siebbeles, *Molecular Simulation* **32**, 695 (2006).
- ⁶ F.C. Grozema, P.T. van Duijnen, Y.A. Berlin, M.A. Ratner, and L.D.A. Siebbeles, *The Journal of Physical Chemistry B* **106**, 7791 (2002).
- ⁷ M. Hultell and S. Stafstroem, *Physical Review B: Condensed Matter and Materials Physics* **75**, 104304/1 (2007).
- ⁸ M. Hultell and S. Stafström, *Physical Review B* **79**, 014302 (2009).
- ⁹ J.C. Tully, *The Journal of Chemical Physics* **137**, 22A301 (2012).
- ¹⁰ T. Nelson, S. Fernandez-Alberti, V. Chernyak, A.E. Roitberg, and S. Tretiak, *The Journal of Chemical Physics* **136**, 054108 (2012).

¹¹ H. Tamura, E.R. Bittner, and I. Burghardt, *The Journal of Chemical Physics* **127**, 034706 (2007).

¹² W. Barford, I. Boczarow, and T. Wharram, *The Journal of Physical Chemistry. A* **115**, 9111 (2011).

¹³ H.L. Chen, Y.F. Huang, T.S. Lim, C.H. Su, P.H. Chen, A.C. Su, K.T. Wong, T.C. Chao, S.I. Chan, and W. Fann, *Journal of Physical Chemistry B* **113**, 8527 (2009).

¹⁴ M.P. Allen, *Molecular Physics* **40**, 1073 (1980).

¹⁵ N.M. Albu and D.J. Yaron, *J. Phys. Chem. C* (submitted) (2013).